IEEE Access
Multidisciplinary | Rapid Review | Open Access Journal

Received November 7, 2021, accepted December 10, 2021, date of publication December 22, 2021,
date of current version January 4, 2022.

Digital Object Identifier 10.1109/ACCESS.2021.3137544

Optimal Management for Megawatt Level Electric Vehicle Charging Stations With a Grid Interface Based on Modular Multilevel Converter

ERDEM GÜMRÜKCÜ[1], (Graduate Student Member, IEEE), EHSAN ASADOLLAHI[1], (Student Member, IEEE), CHARUKESHI JOGLEKAR[1], (Graduate Student Member, IEEE), FERDINANDA PONCI[1], (Senior Member, IEEE), ANTONELLO MONTI[1], (Senior Member, IEEE), GIUSEPPE GUIDI[2], (Senior Member, IEEE), SALVATORE D'ARCO[2], AND JON ARE SUUL[2,3], (Member, IEEE)

[1]Institute for Automation of Complex Power Systems, E.ON ERC—RWTH Aachen University, 52074 Aachen, Germany
[2]SINTEF Energy Research, 7465 Trondheim, Norway
[3]Department of Engineering Cybernetics, Norwegian University of Science and Technology (NTNU), 7465 Trondheim, Norway

Corresponding author: Erdem Gümrükcü (erdem.guemruekcue@eonerc.rwth-aachen.de)

This work was supported in part by the German Federal Ministry of Education and Research (BMBF), and in part by the Research Council of Norway.

ABSTRACT This paper proposes a strategy to manage an electric vehicle charging station (EVCSs) with a grid-side interface based on a Modular Multilevel Converter (MMC). The MMC topology is studied due to its potential for reducing the footprint and the use of active material in the internal distribution system by allowing for transformer-less connection to the medium voltage distribution grid. However, heterogeneous charging demands and arrival-departure profiles of the electric vehicles (EVs) could lead to significant loading unbalances among the MMC arms and among the modules of a single arm. Nevertheless, the current in the grid interface must be kept balanced and sinusoidal. Furthermore, the voltages of the modules of an arm must be balanced. This work combines a load management (LM) algorithm with a power flow management (PFM) algorithm to achieve the required characteristics of grid current and module voltages under the heterogeneity of the charging demand in MMC-based EVCSs. The PFM algorithm controls the circulating currents to compensate the phase-to-phase, arm-to-arm and intra-arm unbalances of the given loading. To minimize the additional losses resulting from active balancing by the PFM, the LM optimizes the charging schedules and allocations of incoming EVs into charging units in order to minimize phase-to-phase and arm-to-arm unbalances in the system. The performance of the proposed optimization-based LM is compared with a rule-based benchmark LM by simulating the daily operation of an example shopping mall parking with MMC-based grid interface. In scenarios with pronounced unbalance limitations, the optimization-based LM increases the supplied energy significantly. Real-time (RT) simulations demonstrate a balanced and sinusoidal grid current profile and balanced module voltages in MMC arms over the daily scenarios. These results indicate that the proposed strategy combining LM and PFM is applicable for real-world deployments.

INDEX TERMS Electric vehicle, modular multilevel converter, optimization, wireless power transfer.

I. INTRODUCTION

With the increasing use of electric vehicles EVs, the availability of charging infrastructures is gaining importance. Due to this trend, large EV charging stations (EVCS) that can deal with the charging needs of hundreds of EVs are planned [1]. Installed power of an EVCS with several hundreds of EV chargers may reach several megawatts. In particular for densely populated urban areas, the compactness of the electrical installation can be crucial. However, most of the

The associate editor coordinating the review of this manuscript and approving it for publication was Behnam Mohammadi-Ivatloo.

available literature studying megawatt-level EVCSs consider the infrastructure requirements for a few fast or ultra-fast DC chargers [2]–[4], where the systems' compactness does not play an important role. One of the few literature examples, which addresses the hardware requirements of a large EVCS, considers a relatively spacious environment such as an airport parking [5].

This paper addresses a special grid interface topology that is particularly interesting for large scale EVCSs in space-constrained urban areas, as it has the potential to significantly reduce the footprint and the requirements for the internal electrical installations. This topology is based on a modular multilevel converter (MMC) where each module supply voltage at floating potential to a single wireless charging unit (WCU) [6]. An overview of the studied configuration is shown in Fig. 1. In such a configuration the overall system load is expected to be unevenly distributed between the arms due to the heterogeneous presence and demand of the hosted EVs. However, for the system to remain connected to public grid, it is necessary to keep the three-phase grid current balanced and sinusoidal despite the loading unbalances between MMC phases and arms. Moreover, loading unbalances between the modules of a single arm may require high circulating currents within the MMC topology to avoid voltage collapse or over-voltage in the MMC modules [6], [7].

It is demonstrated in [6] that limitation of the internal load unbalance can significantly reduce the required circulating currents and the corresponding losses associated with the active balancing control. Furthermore, it is shown in [8] how distribution of a required charging load over a longer period of time also can help to reduce the required balancing effort while leading to increased utilization of the installed power capability of the infrastructure. Thus, it is clear that the operation of the studied EVCS topology can significantly benefit from the implementation of an appropriate load management (LM) strategy.

For other EVCS topologies with similar constraints, previous studies have explored how the temporal flexibility of the load can ease the unbalance problem. For instance, a virtual SOC is introduced in [9], as a metric for representing the aggregated flexibility of a particular MMC arm, which is then utilized for optimizing the power management. However, the previous studies neglect the heterogeneity of the arrival and departure times of the individual EVs in the management and do not consider the possibility to allocate arriving vehicles within the studied topology. Thus, the previously published approaches do not fully utilize the flexibility that can be achieved by LM. To exploit all controllable features, this paper introduces a modified implementation of the optimization-based LM strategy proposed in [10]. This strategy, for simplicity referred to in the following as "optimal LM," optimizes the distribution of the charging load in the MMC arms by controlling the charging schedules and by allocation of an incoming EV to a charging unit within a specific arm. The strategy consists of three

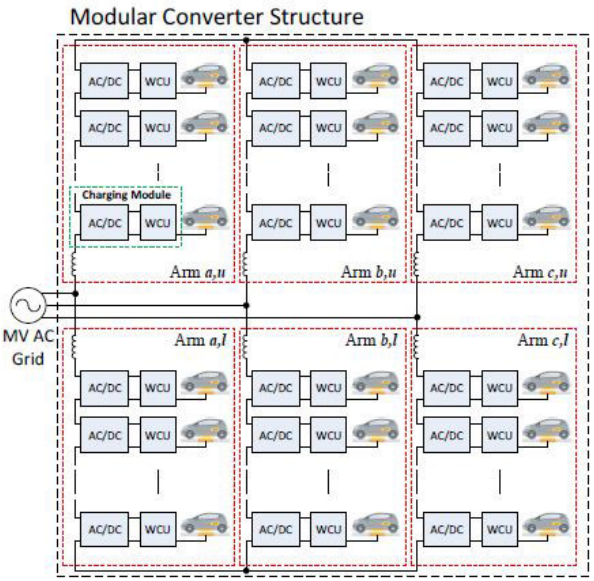

FIGURE 1. Proposed connection layout of large charging infrastructure for wireless EV charging with MMC-based grid interface [6].

optimization models that respectively optimize the charging schedules (optimal scheduling), distribution of the vehicles among the MMC arms (optimal allocation) and short-term power references of the individual charging units (optimal intervention).

The performance of the optimal LM strategy is compared to a rule-based benchmark strategy, which does not optimize the charging profiles and the distribution of EVs into the MMC arms. The comparisons demonstrate that identical scenarios can be handled with smaller phase-to-phase and arm-to-arm unbalances thanks to the optimal LM strategy. As the unbalance that a real system can tolerate would be limited by its current rating and the allowable additional losses due to the balancing control, the unbalance reduction enabled by the optimal LM translates into increased energy supply in identically constrained scenarios. Hence, the proposed strategy promises increased revenue for EVCS operators and higher demand fulfillment rates for EV users.

This study combines the optimal LM strategy with a power flow management (PFM) in a cascaded fashion. For a given event scenario, that is arrival/departures of EVs with certain charging demands, the optimal LM finds the loading scenario that will minimize the phase-to-phase and arm-to-arm unbalances; for the loading scenario given by the optimal LM, the PFM produces the required circulating currents to ensure three-phase balanced and sinusoidal grid current and voltage balance between the modules within the MMC arms. In this paper, the PFM algorithm introduced in [6] is used with the following modification: a look-up table based approach is preferred for calculation of intra-arm balancing. The look-up table contains the optimal values of second harmonic circulating current for a finite number of intra-arm unbalance scenarios. This enables intra-arm

balancing without solving a non-linear optimization problem in real-time.

A real-time (RT) simulation setup is introduced to emulate the system operation of an MMC-based EVCS where both LM and PFM are implemented, and this serves as validation for the proposed management concept. With RT simulations, the capability of the look-up table-based approach for intra-arm balancing is also investigated. The simulation results indicate that the combined LM and PFM management strategy maintains the three-phased balanced grid current and voltage balance in the daily operation of the example shopping mall EVCS scenario and thus validate the practicability of the combined strategy.

The contributions of this work can be summarized as follows. First, all controllable features in an MMC system are exploited in EV charging context. Second, to reduce the computation requirement for calculating the second harmonic component of the circulating current required for handling intra-arm unbalance, a look-up table-based approach is introduced. Third, the overall operation of a controlled system is validated via RT simulations to demonstrate the practicability of the introduced management strategy. To best of the authors' knowledge, this paper presents the first work that exploits all controllable features of an MMC-based EVCS in a LM strategy and validates the practicability of the strategy via RT simulations.

II. CHARGING FACILITY WITH MODULAR CONVERTER BASED GRID INTERFACE

In the reference topology, which is depicted in Fig. 1, the series connection of several LV modules allows for direct connection to distribution systems at medium voltage levels. Each phase of the MMC topology consists of upper and lower arms that are connected between the phase and the positive and negative star-points, respectively.

The topology illustrated in the Fig. 1 relies on EV charging by WCUs based on inductive power transfer, with one charger being supplied by each of the MMC modules. The WCUs are assumed because their inherent galvanic isolation, which will separate the EVs to be charged from the floating electrical potential of the MMC modules [6], [7]. Furthermore, utilization of WCUs can be a preferred solution in terms of user convenience [11] and space coverage in a parking. However, the same topology could also be used for plugged charging units with dedicated galvanic isolation. Thus, the particular technology for charging the individual EVs from the modules of the MMC topology is not within the scope of this work. For the sake of generality we will refer to the charging equipment in the MMC modules as charging units (CUs).

As can be seen in Fig. 1, an MMC-based charging configuration enables transformer-less connection to the distribution grid, and consequently reduces the space requirements and system costs of the large-scale EV charging infrastructure. For the system to remain connected to public grid, it is necessary to keep the three-phase grid current balanced and sinusoidal despite expected loading unbalances between MMC phases and arms. To enable stable grid connection, a proper control strategy is required to ensure balanced grid current while regulating the average value of the capacitor voltage in all the modules. Due to the requirement for handling internal unbalances, the control strategy proposed in [6] could also be easily adapted for operation under unbalanced ac grid voltage conditions, as long as the load can be supplied within the current rating of the grid interface. As the studied topology is in essence a Voltage Source Converter (VSC), the converter can also easily control its ac-side currents under severe grid faults. Thus, the main challenge for protection of the proposed topology against ac-side faults is the design and implementation of strategies for limiting the arm currents to safe values while considering the internal balancing requirements.

Protection of the studied topology against internal faults can be more challenging than protection against grid-side faults. However, previous works such as [7] and [6], recommend to operate the system with a relatively high voltage redundancy. This implies operation with a total available capacitor voltage in each arm that is higher than the peak ac-side voltage. Such a redundancy can also enable handling internal faults in individual MMC modules or CUs, without interrupting the overall system operation thanks to the modular structure. Indeed, any faulted module or CU can be easily bypassed, and a high voltage margin implies that the system can continue operation with one or more faulted modules without the need for increasing the average capacitor voltage.

Since the studied topology is intended for large-scale charging facilities that can accommodate several hundreds of EVs, it also has a significant potential for providing vehicle-to-grid (V2G), or vehicle-to-vehicle (V2V) services. In broader context of V2G functionality, the usual challenges are the lack of standards, cyber-security and battery degradation. In case of an MMC-based system, there exist also topology related challenges. Thus, due to its unbalance limitations, the feasible V2G discharge potential of an MMC-based system can be smaller than the summation of individual discharge potentials of the participating EV batteries. Avoiding such limitations would require over-rating of the installation to allow for the higher circulating currents that would be needed for the internal power balancing control. Nevertheless, in scenarios with highly regular arrival/departure profiles such as residential garages, limitations to the operation due to these constraints can usually be avoided by proper LM. In this paper, though, only unidirectional charging is considered.

III. LOAD MANAGEMENT

For management of MMC-based charging facilities three constraints must be considered. i) The power supplied to each EV is limited due to the nominal power rating of the charging units. ii) The battery capacities of the EVs are limited and state-of-charge (SOC) of the batteries increase during

charging. iii) The circulating currents that compensate phase-to-phase, arm-to-arm and intra-arm unbalances are limited by the system components such as cables and switching devices in the MMC-based electrical installation. Among the mentioned constraints, i) and ii) exist in any EV charging control problem; many authors in the literature proposed alternative techniques such as linear programming [12], stochastic dynamic programming [13], and machine learning [14], all taking into account these constraints. On the other hand, iii) is specific for MMC-based EVCSs. The unbalance limitations determine the power supply capability of the system. Since an EV reaching full SOC affects the load distribution in the system and, thus, the future unbalances, the problem addressed in this work is more complex than most EV charging coordination problems.

The literature provides some references to deal with similar unbalance issues in multi-sectional networks. The authors of [15]–[18] propose scheduling strategies to minimize the three phase unbalances in LV networks with single phase residential connections. However, the MMC-based topology presents a unique problem since not only phase unbalances (horizontal) are problematic but also the unbalances between the arms of the same phase (vertical) and the modules of the same arm (intra-arm).

To limit the complexity in LM, this paper suggests to decouple the overall problem by the same approach considered in [10]. The referenced LM strategy considers a generic topology where CUs in a large EVCS are clustered and clusters are fed through dedicated feeders, each having its own load factor limitation. The strategy optimizes the distribution of the charging load over charger clusters in order to prevent the clusters from local overloading, which occurs while other clusters have a large margin for additional demand. The reference strategy combines three optimization models that, respectively, optimize the charging schedules (optimal scheduling), distribution of the vehicles among the charger clusters (optimal allocation) and short-term power references of charging units (optimal intervention).

In this work, MMC arms are deemed as charger clusters. However, they do not have an inherent load factor constraint as assumed in the referred work. Instead, the unbalances between the MMC arms are operational constraints. Therefore, the strategy from the referred work was modified with additional constraints. In the modified strategy, once an EV arrives in the charging facility, firstly a reference schedule is determined based on the actual and desired SOC, energy capacity of the EV battery and estimated departure time (scheduling). By considering the reference schedules of all EVs in the system, the optimal position (i.e. an MMC module) is selected for the incoming EV (allocation). The scheduling and allocation optimizations are executed sequentially upon the arrival of a single EV. In addition, the LM strategy includes another optimization model that controls the real-time ratings of the chargers considering the individual references of the allocated cars and the unbalance limitations of the MMC (intervention). The intervention model is executed periodically with the actual optimization parameters.

A. OPTIMAL SCHEDULING

When an EV arrives in the charging facility at time t_A, it is assumed that the current state of charge $s^*(t_A)$ and the energy capacity E of the vehicle battery are communicated to the charging station operator (CSO). In addition to $s^*(t_A)$ and E, the user declares an estimate for the departure time t_D. Optionally, the user may specify a target SOC level for the departure $s^*(t_D)$. If $s^*(t_D)$ is not specified, it is assumed that the EV owner aims at 100% SOC. In this work, it is assumed that all mentioned parameters are accurately known.

With the given parameters, the CSO calculates the reference schedules $p^* = (\,p^*(t)\; p^*(t+\Delta t)\; \ldots\,)^T$ over a scheduling horizon $t \in [t_A, t_D)$ discretized by Δt. In the vector p^*, each $p^*(t)$ is an optimization variable that represents the power to be supplied to the EV at a time interval t. The scheduling optimization produces also the reference SOCs for particular t steps, $s^*(t)$, which are in effect dependent upon p^*:

$$0.0 \leq p^*(t) \leq P_C \tag{1}$$

$$s^*(t+\Delta t) = s^*(t) + \frac{p^*(t) \cdot \eta \cdot \Delta t}{E} \tag{2}$$

$$0.0 \leq s^*(t) \leq 1.0 \tag{3}$$

It is assumed that the CUs in each MMC module have the capability of modulating power between 0 and its power rating, P_C. The supply capability of a charger is expressed with the constraint (1). In (2)-(3), $s^*(t+\Delta t)$ and $s^*(t)$ represent the SOC in successive time intervals. (2) and (3) ensure respectively that SOC increases according to the supplied energy at each time interval and that energy capacity of the EV battery is respected. With the given charger rating and time, the SOC must be increased from $s^*(t_A)$ to $s^*(t_D)$.

The optimization objective of the schedules problem is minimizing the charging cost. Therefore, the power is weighted with the time-depending electricity price $\kappa(t)$ in the objective function:

$$min \sum_{t=t_A}^{t_D} \kappa(t) \cdot p^*(t) \tag{4}$$

The calculated p^* and s^* are passed over to the optimal allocation model as optimization parameters.

B. OPTIMAL ALLOCATION

The relationship between the circulating current and the horizontal, vertical and intra-arm unbalances are highly nonlinear. In order to build a scalable optimal allocation model two assumptions were considered. First, the impact of the intra-arm unbalances can be neglected in allocation decisions because the proper voltage redundancy in the MMC arms enables module voltage stability independently from the intra-arm distribution of the load. Second, the principle that the less unbalance leads to the less circulating current applies almost always; the local exceptions to this rule occur

rather temporarily without affecting long-term operational objectives of the system and, thus, can be neglected.

Based on the aforementioned assumptions, the allocation model that was presented in the previous work of the authors [19] was adopted. The adopted model neglects intra-arm unbalances and considers only the power unbalance between the phases (horizontal) and the arms of each phase (vertical) as the system constraints rather than the circulating currents. The reference schedules p^* calculated through (1)-(4), are used as optimization parameters in the allocation problem. With l indexing the leg (phase), a the arm and n the module, a particular MMC module is represented by l, a, n. Since the position in a particular arm does not affect the horizontal and vertical unbalances, the allocation options are represented by six binary variables $x_{l,a}$, each indicating allocation a particular arm:

$$\sum_{l=1}^{3}\sum_{a=1}^{2} x_{l,a} = 1 \tag{5}$$

$$x_{l,a} + I_{l,a} \leq N \tag{6}$$

Above (5) ensures allocation to only one of the MMC arms. $I_{l,a}$ is an integer parameter which indicates the number of connected EVs in the arm l, a. With N representing the number of modules in an arm, (6) ensures that the incoming EV is sent to an MMC arm with a vacant module. With $p^*_{l,a,n}(t)$ being the reference schedule of the EV connected in the module l, a, n and $p^*(t)$ the schedule of the incoming EV, the arm power and power become respectively $p^*_{l,a}(t)$ and $p^*_l(t)$ after the allocation:

$$p^*_{l,a}(t) = p^*(t) \cdot x_{l,a} + \sum_{n=1}^{N} p^*_{l,a,n} \tag{7}$$

$$p^*_l(t) = p^*_{l,1}(t) + p^*_{l,2}(t) \tag{8}$$

The objective of the optimization model is the minimization of the total cumulative unbalance of the system over the optimization horizon $t \in [0, T)$. The unbalance term $u = (\,u(t)\ u(t+\Delta t)\ \ldots\ u(T-\Delta t)\,)^T$, aggregates the total vertical unbalances (the load difference between upper and lower arms of the phases) and horizontal unbalances (the load difference between the phases of the MMC:

$$u = \sum_{l=1}^{3} \mid p^*_{l,1} - p^*_{l,2} \mid + \sum_{l_1 \neq l_2 \in \{1,2,3\}} \mid p^*_{l_1} - p^*_{l_2} \mid \tag{9}$$

$$min \sum_{t=0}^{T} u(t) \tag{10}$$

By solving the optimal allocation problem, the MMC arm to allocate the incoming EV is identified. Since the position in a particular arm does not affect the horizontal and vertical unbalances, a random module is selected to connect the EV. After module selection, the reference SOC $s*$ calculated for the incoming EV at the scheduling step becomes the reference SOC of the connected MMC module, $s^*_{l,a,n}$.

C. OPTIMAL INTERVENTION

The model for the optimal intervention is, in essence, a reference tracking algorithm that enforces the unbalance constraints of the MMC while adjusting the charging rates of all CUs in the real-time operation. These adjustments ensure that the loading unbalance is always kept within the tolerable limits while the references schedules are tracked as long as possible. The optimal intervention problem is formulated as a model predictive control (MPC) problem. In this problem real time charging rates of the MMC modules, $p_{l,a,n}(t)$, are the main control variables and the SOCs of the connected cars, $s_{l,a,n}(t)$, are the state variables which evolve according to $p_{l,a,n}(t)$ and the energy capacity of the EV batteries, $E_{l,a,n}$:

$$s_{l,a,n}(t + \Delta t) = s_{l,a,n}(t) + \frac{p_{l,a,n}(t) \cdot \eta \cdot \Delta t}{E_{l,a,n}} \tag{11}$$

$soc_{l,a,n}(t)$ variables are upper and lower bounded with the same constraint as given in (2). Equation (1) was modified slightly in order to limit the charging power of the MMC modules with respect to presence of the connected cars. $B_{l,a,n}(t)$ is the binary presence parameter that has the value of 1 at the time steps before the departure t_D of the connected car and 0 at the later time steps:

$$0.0 \leq p_{l,a,n}(t) \leq B_{l,a,n}(t) \cdot P_C \tag{12}$$

The individual module powers aggregate into the arm, $p_{l,a}(t)$, and phase $p_l(t)$ powers, as shown in (13-20). The vertical and horizontal unbalance constraints, (15-16), are expressed in normalized terms with respect to the arm and power capacities. For example, the selection ($\beta = 10\%$) means that the system is allowed to tolerate vertical and horizontal unbalance up to 10% of the arm and phase power capacities respectively:

$$p_{l,a}(t) = \sum_{n=1}^{N} p_{l,a,n}(t) \tag{13}$$

$$p_l(t) = p_{l,1}(t) + p_{l,2}(t) \tag{14}$$

$$-\beta \cdot N \cdot P_C \leq p_{l,1}(t) - p_{l,2}(t) \leq \beta \cdot N \cdot P_C \tag{15}$$

$$-\beta \cdot 2N \cdot P_C \leq p_l(t) - p_m(t) \leq \beta \cdot 2N \cdot P_C \tag{16}$$

It is important to note that variations in the efficiency of the converter in each module and the corresponding charging units due to the operating point are neglected in the control model. Therefore, it is assumed that the system can perfectly transfer any calculated $p_{l,a,n}(t)$ as long as the unbalance constraints are respected.

The objective function consists of as many elements as the number of modules in the MMC system. This function models the deviation from the reference SOC schedules separately at the individual level while penalizing the aggregated deviation from the reference schedules s^* at the end of an optimization horizon T:

$$min \sum_{l=1}^{3}\sum_{a=1}^{2}\sum_{n=1}^{N} \left| s^*_{l,a,n}(T) - s_{l,a,n}(T) \right| \tag{17}$$

where $s^*_{l,a,n}(t)$ is the reference SOC of the EV connected to the module l, a, n at a time interval t.

IV. POWER FLOW MANAGEMENT

This section introduces the methodology to achieve three-phase balanced and sinusoidal grid currents and voltage balancing among all the modules of the three phase MMC charging infrastructure. The circulating current can be controlled independently in each phase and is composed of dc-, fundamental frequency and second harmonic frequency components. These components enable compensation of horizontal, vertical, and intra-arm unbalances respectively.

As commonly preferred in MMC literature, such as [20], this paper utilizes Σ and Δ notations to simplify mathematical expression of the control variables and interpretation of the balancing requirements. Thus, the loading of the studied topology is expressed by:

$$p_l^{\Sigma} = \frac{p_{l,1} + p_{l,2}}{2} \tag{18}$$

$$p_l^{\Delta} = \frac{p_{l,1} - p_{l,2}}{2} \tag{19}$$

where $p_{l,1}$ and $p_{l,2}$ indicate, respectively, the power of the upper and lower arms of phase l. For the sake of simplicity, the terms are referred to as Σ and Δ components of the respective quantities such that p_l^{Σ} is mentioned as the Σ component of the phase power of l.

A. COMPENSATION OF HORIZONTAL UNBALANCE

Compensation of horizontal unbalance can be achieved by introduction of a dc circulating current [21], [22]. Assuming balanced grid voltages, the power absorbed from the grid should be divided equally between the three phases. In case of a power mismatch between the three phases, a dc circulating current is required to compensate the horizontal unbalance:

$$i_l^{dc} = \frac{\sum_{a=1}^{2} p_{l,a} - 1/3 \sum_{l=1}^{3} \sum_{a=1}^{2} p_{l,a}}{2 \sum_{a=1}^{2} v_{l,a}} \tag{20}$$

In this equation, $v_{l,a}$ is the voltage of the associated arm. The sum of dc components of the three phases is equal to zero, since the studied topology does not have a DC link terminal. Therefore, the dc component of circulating current allows the power to be transferred from one phase (leg) to another. It can be interpreted from equation (20), that distributing the load equally between the three phases will minimize the required dc component of circulating current.

B. COMPENSATION OF VERTICAL UNBALANCE

Compensation of vertical unbalances requires independent power flow between upper and lower arms of each phase. The fundamental frequency component of the circulating current enables power exchange between the upper and lower phase arms. In [6], the fundamental frequency components required for compensating given vertical unbalances is defined as a function of aggregated arm powers $p_{l,a}$. The referred work applies Σ/Δ notations to derive the expression for required fundamental frequency component in terms of symmetrical components as follows:

$$Re(i^{\Sigma}_{+\omega}) = -\frac{1}{\hat{v}_g} \cdot \frac{p_1^{\Delta} + p_2^{\Delta} + p_3^{\Delta}}{3} \tag{21}$$

$$Re(i^{\Sigma}_{-\omega}) = -\frac{1}{\hat{v}_g} \cdot \frac{2p_1^{\Delta} - (p_2^{\Delta} + p_3^{\Delta})}{3} \tag{22}$$

$$Im(i^{\Sigma}_{-\omega}) = \frac{1}{\hat{v}_g} \cdot \frac{1}{\sqrt{3}} \cdot (p_2^{\Delta} - p_3^{\Delta}) \tag{23}$$

where $i^{\Sigma}_{+\omega}$ and $i^{\Sigma}_{-\omega}$, respectively, represent positive and negative sequence components of fundamental frequency circulating current. The equation (21) indicates that the real part of the fundamental frequency positive sequence circulating current, $Re(i^{\Sigma}_{+\omega})$, relates to the overall vertical unbalance in the system. From (22) and (23), it follows that the real $Re(i^{\Sigma}_{+\omega})$ and imaginary parts $Im(i^{\Sigma}_{+\omega})$ of the fundamental frequency negative sequence circulating current compensate the vertical unbalances in different phases.

C. INTRA-ARM CAPACITOR VOLTAGE BALANCING

According to [6], for the average voltage across the module capacitors to remain stable, following condition must hold:

$$\frac{1}{T_i} \int_0^{T_i} \frac{i_{l,a} + |i_{l,a}|}{2} . dt \geq k_m . \frac{p^M_{l,a}}{v_{l,a}} \tag{24}$$

where is T_i the fundamental period. Within T_i the module loads are assumed to be constant. In this equation, k_m is the necessary redundancy factor that serves as a safety margin for the non-modeled losses and the delays in the control. $p^M_{l,a}$ is the maximum load of the modules in arm l, a and $v_{l,a}$ the DC-link voltage. With $i_{l,a}$ being the arm current, $\frac{i_{l,a}+|i_{l,a}|}{2}$ in (24) represents the positive values of the arm current with an ideal insertion index, which only allows charging current to flow into the capacitor from ac-side to the dc-side.

In most MMC applications such as [23], conventional sorting algorithms can guarantee nominally identical capacitor voltages. However, in the studied application, modules within a single arm can have considerably different loading. To ensure the condition in (24) is fulfilled, the authors of [6] propose to add a second harmonic component $i_{l,2\omega}$ to the arm current as follows:

$$i_{l,a}(t) = i_{l,dc} + Re(i_{l,a,\omega} \cdot e^{j\omega t}) + Re(i_{l,2\omega} \cdot e^{j2\omega t}) \tag{25}$$

In certain cases, when the arms are highly loaded, the dc and fundamental frequency components are sufficient to satisfy the charge balance equation (24). However, when the intra-arm unbalances are significant, an additional second harmonic current needs to be injected to fulfill the necessary voltage stability condition. Since $i_{l,2\omega}$ leads to losses during the operation, the intra-arm balancing problem is defined as

an optimization problem:

$$minf(\mathbf{x}) = \sum_{l=1}^{3} \int_{0}^{T_i} |i_{l,2\omega}(t).dt| \tag{26}$$

$$\mathbf{x} = [i_{l,2\omega}] = [Re(i_{l,2\omega}), Im(i_{l,2\omega})] \tag{27}$$

$$\mathbf{p} = [p_{l,a}, p_{l,a}^{M}] \tag{28}$$

$$\sum_{l=1}^{3} Re(i_{l,2\omega}) = 0 \tag{29}$$

$$\sum_{l=1}^{3} Im(i_{l,2\omega}) = 0 \tag{30}$$

In the optimization model (26)-(30), $f(x)$ is the objective function minimizing the absolute value of total second harmonic current, and $\mathbf{x}$ represents the optimization variables comprising of the real $Re(i_{l,2\omega})$ and imaginary $Im(i_{l,2\omega})$ parts of the second harmonic current of each phase. The optimization problem is a function of twelve parameters in $\mathbf{p}$, including the aggregated power of each arm and the maximum existing load power in each arm.

By representing the necessary condition for module voltage stability with the maximum load in each arm, the rule (24) fulfills the stability condition for the rest of the modules within the arm. Therefore, the inequality (24) is an optimization constraint. The equality constraints (29) and (30) enforce Kirchhoff current law for the real and imaginary part of the second harmonic circulating current.

This convex optimization problem can be solved using interior point method. However, by taking into account the computation power constraints, this paper applies a look-up table based approach to calculate required second harmonic components in the real-time operation. The details of the implementation of circulating current control is presented in section V alongside with the real-time simulation setup.

V. REAL-TIME SIMULATION SETUP

The modular charging system of Fig. 1 was first modeled in MATLAB-Simulink. This model was then split into multiple subsystems so as to be compatible for simulations in real-time using the real-time digital simulator OP5707 from OPAL-RT [24]. For the purpose of real-time simulation, the model has been split into four subsystems including the Graphical User Interface (GUI) subsystem and the three computational subsystems consisting of the control, modulation and electrical circuit subsystems. The MMC and the MV grid is modelled in the electric subsystem. Each computational subsystem is executed in real-time on one of the Central Processing Unit (CPU) cores of the real-time digital simulator target OP5707. Data exchange between computational subsystems is synchronous through shared memory and it is asynchronous between the GUI subsystem and computational subsystems. Figure 2 shows the aforementioned subsystems of the simulation.

Computational subsystems are executed with a fixed time-step and in order for the simulation to be executed in real-time, the simulation output from each of the computational subsystems should be available for the rest of the computational subsystems by the end of this fixed time step. A longer computation time than the associated time step will result in loss of data.

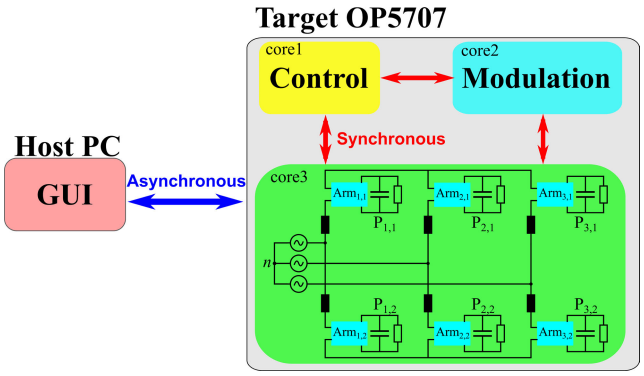

FIGURE 2. Overview of real-time simulation model subsystems.

The electrical circuit subsystem, specifically the MMC and its switching frequency limit the maximum time step. For real-time simulation to be feasible, the computation time in modulation and control subsystems must be smaller than this limit. The computation tasks performed by the modulation subsystem are not computationally complex and thus, do not influence the selection of the time step. In the control subsystem, two of the functions, dc and fundamental frequency component calculations are relatively trivial. However, the second harmonic component is calculated by solving a non-linear optimization problem, which may require long computation times in certain loading scenarios.

Selection of a constant time-step that is sufficiently large to calculate the required second harmonic current in all possible scenarios would require a very large time step and this might be an hindrance to simulate the system in real-time. Therefore, to achieve a small and comparatively constant computation time for different arm loading values in the real-time operation, a look-up table was deployed that contains the optimal values of second harmonic circulating current for a finite number of states i.e. MMC loading scenarios. To generate the look-up table, N^{opt} number of optimization problems have to be solved offline:

$$N^{opt} = (k_1 \times k_2)^6 \tag{31}$$

In (31), k_1 is the number of discretized states of each input loading power parameter of the look-up table and k_2 is the number of discretized states of maximum module power for each arm. As stated in Section IV-C, the optimal values of the second harmonic components depend on 12 input parameters: $p_{l,a}$ and $p_{l,a}^{M}$ of each arm. To decrease the required N^{opt}, we assume a constant $p_{l,a}^{M}$ of $1pu$ in (24), which represents the worst case scenario, i.e. a scenario in which the maximum second harmonic component of the circulating current is required to be compensated. This selection ensures that,

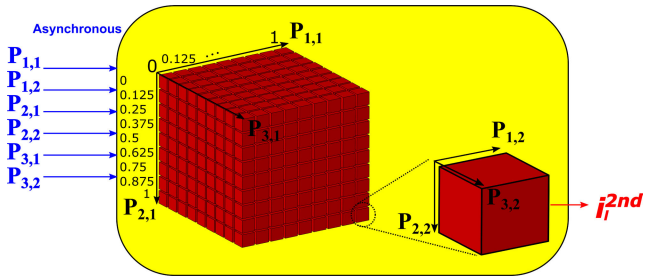

FIGURE 3. Look-up table visualisation.

despite some inefficiencies in the operation, module voltages are kept stable in all loading scenarios. When $p_{l,a}^{M}$ are removed from the optimization problem, (28) and (31) reduce to the following respectively:

$$\mathbf{p} = [p_{l,a}^{\Sigma}] \tag{32}$$

$$N^{opt} = k_1^6 \tag{33}$$

In this selection, the look-up table is a 6-dimensional (6D) matrix. For the sake of visualization, Figure 3 illustrates the structure of the look-up table as two nested cubes (3D matrices), where the outer cube represents the states of upper arm powers $p_{l,1}$ and inner cube for lower arm powers $p_{l,2}$.

It is important to note that, in theory, there exist an infinite number of states in the continuous operating range of MMC modules while a look-up table can only contain a finite number of states. The optimal second harmonic values for the non-simulated operating points, which reside between two states in the look-up tables, are interpolated with nearest neighbor interpolation method [25]. This method assigns the output value of an input, that is not among the pre-calculated input states to the nearest data point that exists in the look-up table. This method does not necessarily provide the most accurate interpolated value for each scenario but as it inherently removes the risk of diverging from the optimized curve, it is found to be a robust method for this application.

Deploying a look-up table in the control subsystem rather than having to solve optimization problems makes it possible to obtain the required second harmonic currents in significantly shorter time period, allowing for the real-time simulation of the systems with larger scales. On the other hand, such simplification results in higher second harmonic injection than the optimal value, which could be obtained by solving the original optimization problem (26)-(28) in certain cases.

Figure 4 shows the difference between the second harmonic current calculated by the optimization and interpolated values from the look-up table with nearest neighbor interpolation method for a sample case of $\mathbf{p}$. In the tested case, the loading of all arms except $p_{1,1}$ are kept constant at certain pu values and the value of $p_{1,1}$ is varied within $0 \leq p_{1,1} \leq 1pu$ such that $\mathbf{p} = [p_{1,1}, 0.1, 0.2, 0, 0.5, 0.7]$. The dashed line shows the optimized value and the continuous line shows the interpolated values. As can be seen in this figure, the interpolated second harmonic value deviates slightly from the values obtained by solving the optimization problem. In section VII, it is demonstrated that the look-up table based second harmonic values can still ensure module voltage stability.

TABLE 1. Summary of the charging system parameters.

Parameters of the simulated MMC	
Nominal line-to-line grid voltage	22 000 V rms
Total installed power	6.6 MW
Number of charging modules	300
Number of charging modules per arm	50
Arm DC voltage	60 000 V
Module voltage	1200 V
Module nominal load	22 kW
Module Capacitance	1.7 mF

VI. TEST SCENARIO

A. USE CASE SPECIFICATION

We tested the proposed management strategy in a scenario taking place in an example shopping mall parking on a Saturday. The tested scenario was generated by sampling 542 EVs from hypothetical models ModelA, ModelB, ModelC with respectively 55 ,40 and 32 kWh battery capacities; the batteries of these models can be charged with maximum 22 ,12 and 7 kW power respectively. Random arrival and departure times were assigned to each EV such that their parking duration ranges between 2-4 hours. The generated scenario starts with a vacant parking; the first EV arrives at 12:00 and the last one leaves at 21:05. In this period, each EV visits the parking only once with an arrival SOC ranging between 40%-90%.

B. TOPOLOGY PARAMETERS AND SIMULATION MODELS

A charging infrastructure that consists of 300 MMC modules (50 per arm) is considered in the simulations. Each of the EV chargers have 22 kW power rating. Table 1 summarizes the parameters of the considered electrical installation.

The scenarios are simulated in Python by neglecting the uncertainties in SOC measurement of the EV batteries and considering that the SOCs increase according to (11) as long the power rating of the chargers are respected. Furthermore, the arm power equations (13) are considered to hold true as long as the unbalance stays in the limits defined by the tolerance β.

C. IMPLEMENTATION OF THE OPTIMIZATION MODELS

The optimization models are implemented by using the library Pyomo [26]. In the simulated cases, the time discretization, Δt, of 5 min is selected for all three optimization models. The optimization horizon for optimal allocation problem in these tests are 4 hours as it is the maximum parking duration of the EVs in the shopping mall park. The horizon for optimal intervention is limited by 1 hour since the

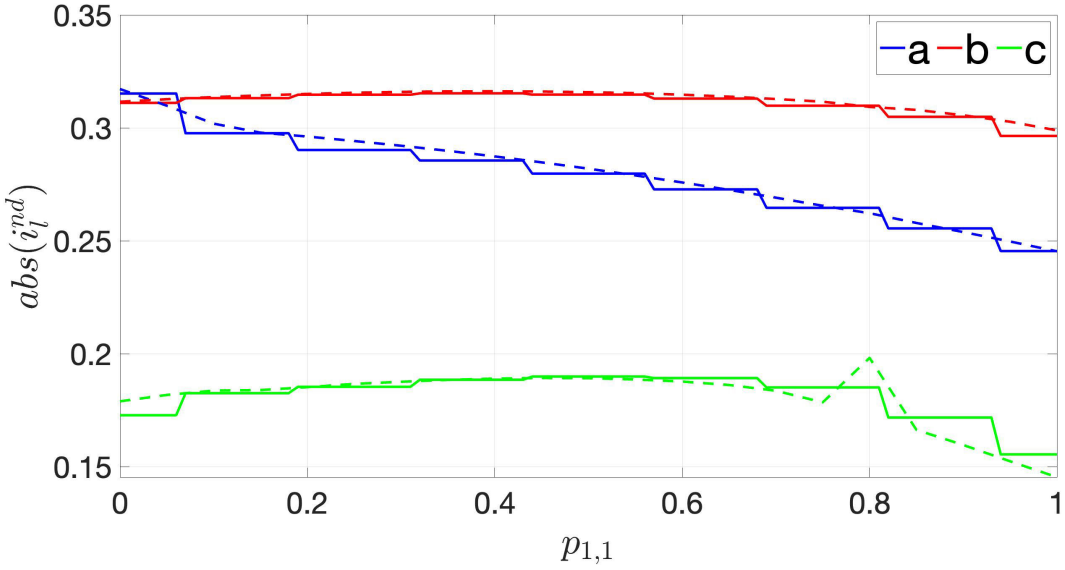

FIGURE 4. Comparison of optimized and interpolated second harmonic current amplitude.

given conditions can significantly change by the introduction of new cars in the system in few hours. The problems are solved by using the optimization solver CPLEX [27].

D. BENCHMARK LM AND PERFORMANCE METRIC FOR EVALUATION OF THE PROPOSED LM

In the following sections the performance of the proposed optimization-based LM is evaluated. For the sake of simplicity, this strategy is referred to as optimal LM (O-LM) in the discussions. This section defines a benchmark LM (B-LM) strategy to evaluate the performance of O-LM.

The B-LM is a rule-based strategy. In B-LM, the charging profiles are not scheduled and therefore, the EVs start charging immediately after the connection. An incoming EV is allocated to one of the modules in the arm that accommodates the least number of EVs at the moment of arrival. It is important to note that, unlike the O-LM, the B-LM takes the allocation decisions without considering the future loading. Likewise, the B-LM does not have a forward-looking selective approach to intervene the load when the unscheduled charging denotes an unbalance that exceeds the tolerable limit β. In this case, the power of the arms that cause excessive unbalance are reduced by modulating each module with the same factor without distinguishing the demands and departures of the connected EVs.

To quantify the performance of alternative LM approaches we define a metric e^{σ} that measures the cumulative energy that is transferred to the EV batteries in a given scenario taking place within a simulation horizon of $[t_0, t_F]$:

$$e^{\sigma} = \sum_{t=t_0}^{t=t_F} \sum_{l=1}^{3} \sum_{a=1}^{2} \sum_{n=1}^{N} p_{l,a,n}(t) \cdot \eta \cdot \Delta T \qquad (34)$$

VII. SIMULATION RESULTS

A. NUMERICAL SIMULATIONS

To investigate the impact of applied LM strategy on loading unbalances, we analyzed the arm and phase power profiles by applying both benchmark and optimal LM in the scenario that is introduced in Section VI-A. For this analysis, we allowed unlimited horizontal and vertical unbalances in the simulations by selecting $\beta = 100\%$ in (15) and (16). The resulting powers of the MMC arms in benchmark and optimal LM cases are plotted in Fig. 5. Fig. 6 and 7 depict, respectively, the absolute values of the horizontal and vertical unbalances observed in these simulations.

According to the simulation results, when B-LM is applied, the horizontal unbalance between phases often exceeds 100 kW reaching 214 kW (between phases 1 and 3) at 14:50. On the other hand, the maximum unbalance between two phases observed in O-LM is 58 kW. Likewise, the O-LM keeps the vertical unbalance always under 55 kW whereas the vertical unbalance exceeds 110 kW several times in B-LM. The simulation results illustrated in Fig. 6 and Fig. 7 denote the clear superiority of O-LM over B-LM in terms of loading unbalance. In a real-world deployment, the balancing capability of an MMC system is determined by the switching devices and cables; unbalances exceeding the system capabilities are rejected in order to maintain the balanced grid current. Therefore, unbalance reduction can translate into an increase in supplied energy. To evaluate the impact the optimal LM in this aspect, we applied it in scenarios with pronounced unbalance limitations.

To quantify the performance in an objective way, we compared energy supplied by B-LM and O-LM in large number of scenarios. To this end, we modified the original scenario presented in Section VI-A by shifting the arrivals/departures

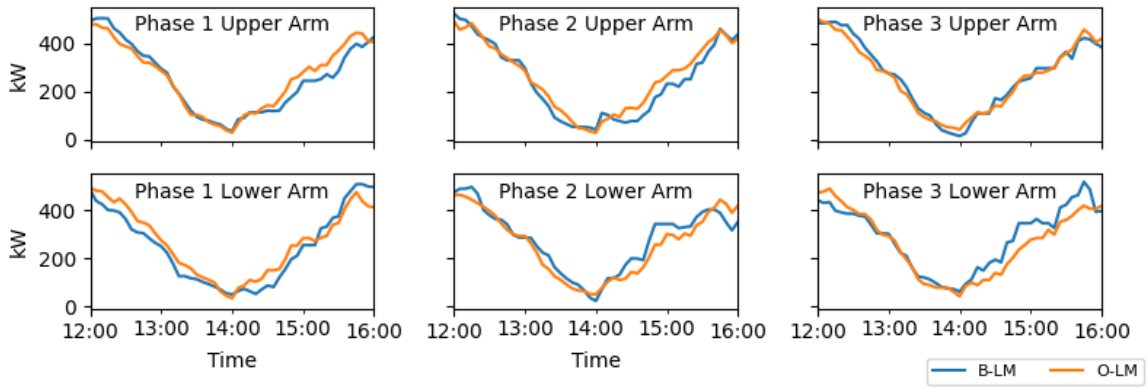

FIGURE 5. Arm powers in B-LM and O-LM.

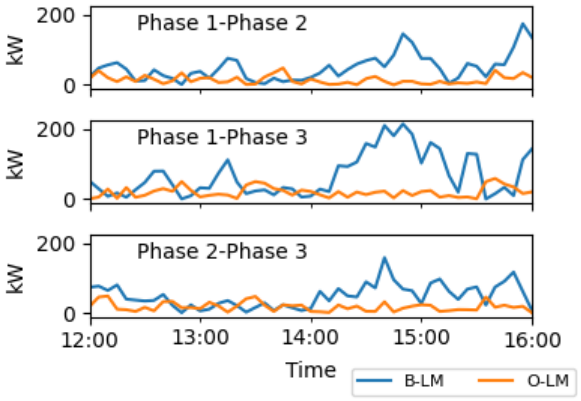

FIGURE 6. Horizontal unbalances in B-LM and O-LM.

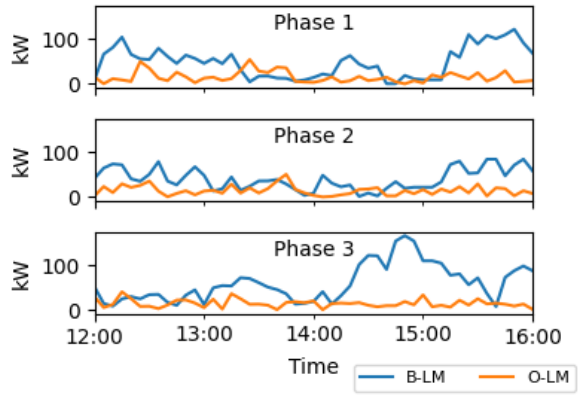

FIGURE 7. Vertical unbalances in B-LM and O-LM.

of randomly selected EVs by ±5 minutes without changing the arrival/target SOC and parking duration. 100 unique but similar scenarios were obtained through these modifications. These scenarios are referred to as modified scenarios in the discussions. We simulated each modified scenario for the selection of $\beta = 0\%$ and $\beta = 2\%$. It is important to note that the selection $\beta = 0\%$ indicates the requirement of a strict balancing between MMC-arms. In $\beta = 2\%$, the maximum allowed arm-to-arm unbalances is 1/50 of the installed power of an MMC arm, which accounts for the power rating of a single CU in our scenario.

The comparisons indicate that, in scenarios under 0% unbalance tolerance condition, O-LM gives 2%-15% rise to the supplied energy. The impact of selected management strategy on e^{σ} gradually decreases with the relaxation in unbalance tolerance. Under $\beta = 2\%$ in 73% of the scenarios, the O-LM enables 1-3% supply increase; in the rest of the scenarios the improvement is within 3-5%. Figure 8 shows the histograms of cumulative energy supply in 100 modified scenarios for two cases where unbalance is critically constrained i.e. $\beta = 0\%$ and $\beta = 2\%$. In the zero-tolerance to unbalance case, which is shown in Figure 8(a), the frequency distribution of B-LM is relatively symmetrical; on the other hand, the graph of O-LM is highly skewed to the right. The histograms of both strategies for $\beta = 2\%$ case, Figure 8(b), are concentrated into high supply intervals. Nevertheless, the supply in B-LM ranges between 9450-9850 kWh interval while it is always within 9850-9900 kWh range in O-LM. These results indicate that the performance B-LM is affected significantly when the arrival/departure times shift by ±5 minutes whereas the O-LM's response is greatly uniform under such variations.

The numerical simulations show that the benchmark LM can guarantee 9900 kWh energy supply in all scenarios in case of $\beta = 10\%$ -which optimal LM guarantees in case of $\beta = 2\%$. In practice, larger unbalance tolerance can be obtained only through a corresponding over-sizing of system components such as larger cable cross-sections. Therefore, these results also clarify the importance of the LM strategy for the system sizing and investment costs.

B. REAL-TIME SIMULATIONS

To demonstrate that the optimal LM is suitable to operate the MMC-based EVCS, we applied it together with PFM that controls the circulating currents to achieve three phase balanced and sinusoidal grid current and module voltage stability. With the setup depicted in Fig. 2, we performed RT simulations for the case that allows for 10% vertical and horizontal unbalances. The reason underlying this selection

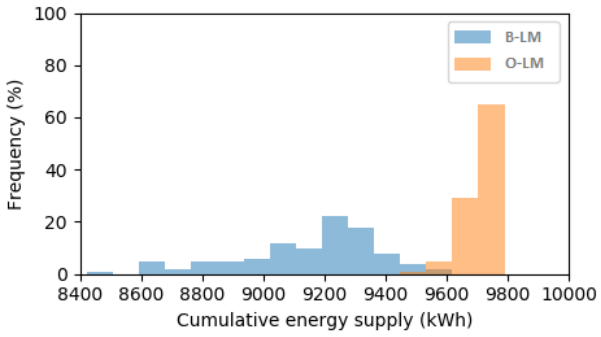

(a) Unbalance tolerance $\beta = 0\%$

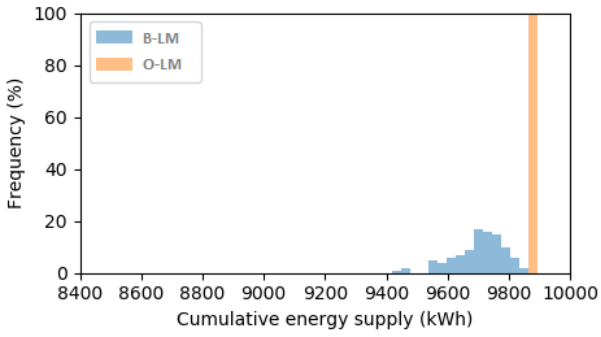

(b) Unbalance tolerance $\beta = 2\%$

FIGURE 8. Energy supply histograms in 100 modified scenarios.

is to test the function of PFM in a scenario where loading unbalances can be significant. In RT-simulations, we investigated the intra-arm balancing capability (i.e. module voltage stabilization) of the look-up table approach as well as the horizontal and vertical balancing capability of the PFM algorithm. To this end, we compared the scenarios i) without injection of the second harmonic circulating current versus ii) with second harmonic current calculated by using the look-up tables.

Fig. 9 shows the minimum module voltages observed in RT-simulations. As can be seen in Fig. 9(a), without proper injection of the second harmonic circulating current, the module voltages frequently drop to zero. Clearly, the system is not operable in this case. On the other hand, when the intra-arm a second harmonic current specified by the look-up table is injected, the PFM guarantees the stability of module voltages in each arm as illustrated in Fig. 9(b).

We investigated the impact of the system operation in fully controlled scenario -with LM controlling load and PFM algorithm compensating the unbalances- on the current drawn from the MV grid. The grid current wave-forms, I_{abc}, are observed in the RT simulations. Fig. 10 depicts the daily profiles of the currents drawn by the MMC from the grid. Identical amplitude of the three phases of the grid currents throughout the simulation horizon verifies the function of horizontal and vertical load balancing controls. To observe the wave-forms of the grid current and voltage, we plotted the observed values of these quantities for few

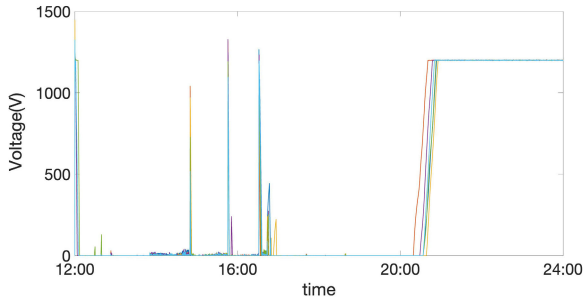

(a) Without second harmonic circulating current control

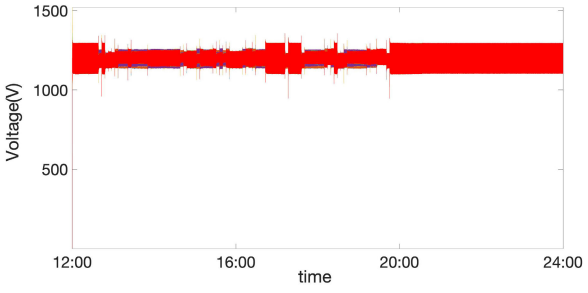

(b) With second harmonic circulating current control

FIGURE 9. Minimum module voltage.

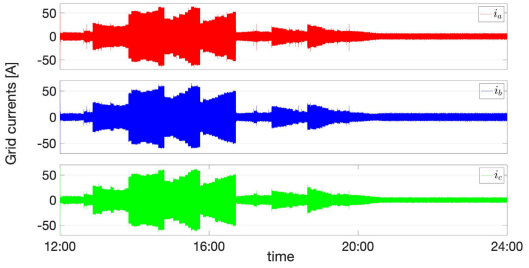

FIGURE 10. Grid current in each phase of the grid in daily operation of MMC-based EVCS.

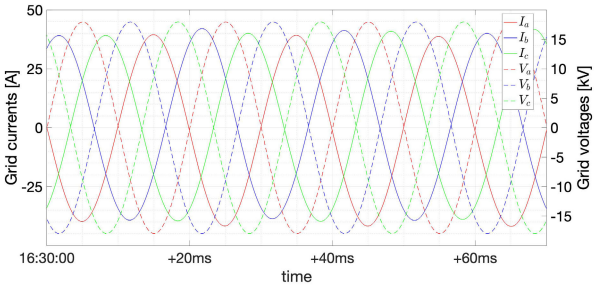

FIGURE 11. Wave-forms of the grid current and voltage for few fundamental periods in highly unbalanced case.

fundamental periods after 16:30 where the highest unbalance load occurs in the O-LM scenario. The perfectly balanced sinusoidal current wave-form depicted in Fig. 11 demonstrate the balancing capability of the PFM.

VIII. CONCLUSION

This paper presents a load management (LM) strategy for the large-scale electric vehicle (EV) stations with a grid-side interface based on a modular multilevel converter (MMC)

topology. In this strategy, the charging profile of an incoming EV is optimized with the goal of charging cost minimization (optimal scheduling). Based on this schedule, the EV is allocated to an MMC arm in a way that minimizes horizontal (between MMC phases) and vertical (between arms of the same phase) unbalances over a future horizon (optimal allocation). During the operation, the system tracks the schedules set forth by optimal scheduling under the unbalance constraints of the MMC considering (optimal intervention).

To assess the performance of the proposed LM strategy, several scenarios representing the operation of a typical shopping mall parking facility are generated and simulated. The results obtained in these simulations are compared with those of a benchmark LM approach, which does not control the schedules and allocates the EVs to the arms with minimum number of connected EVs without considering the loading unbalances. The comparisons show that optimal LM reduces vertical and horizontal unbalances significantly. Thanks to the unbalance reduction enabled by the optimal LM, the supply potential of the system increases by up-to 15% in certain scenarios where the system rejects all horizontal and vertical unbalances. Furthermore, optimal LM prove to respond consistently to nearly identical scenarios while the benchmark LM's performance can show a great variability under small changes in the scenario. e.g. ± 5 minutes of shifts in connection events.

To demonstrate that the strategy can be implemented in a practical system, real-time simulations are performed. In these simulations, the optimal LM strategy determines the loading of the MMC arms while a power flow management algorithm controlling the internal power flows between and within MMC arms ensures that the current drawn from the public three phase grid is balanced and sinusoidal and the MMC module voltages are stable. The real-time simulation results indicate that the proposed strategy is applicable to manage the charging operations in a shopping mall or other scenarios with highly random behavior of the EVs.

ACKNOWLEDGMENT

Modular Megawatt-Range Wireless EV Charging Infrastructure Providing Smart Grid Services (MoMeWeC) is a research project of the international joint initiative EIG CONCERT, Japan, under the Joint Call on Efficient Energy Storage and Distribution.

REFERENCES

[1] B. Wang, P. Dehghanian, S. Wang, and M. Mitolo, "Electrical safety considerations in large-scale electric vehicle charging stations," *IEEE Trans. Ind. Appl.*, vol. 55, no. 6, pp. 6603–6612, Nov. 2019.

[2] H. Tu, H. Feng, S. Srdic, and S. Lukic, "Extreme fast charging of electric vehicles: A technology overview," *IEEE Trans. Transport. Electrific.*, vol. 5, no. 4, pp. 861–878, Dec. 2019.

[3] T. He, J. Zhu, D. Dah-Chuan Lu, L. Zheng, M. M. Aghdam, and J. Zhang, "Comparison study of electric vehicles charging stations with AC and DC buses for bidirectional power flow in smart car parks," in *Proc. 43rd Annu. Conf. IEEE Ind. Electron. Soc. (IECON)*, Oct. 2017, pp. 4609–4614.

[4] M. Tabari and A. Yazdani, "An energy management strategy for a DC distribution system for power system integration of plug-in electric vehicles," *IEEE Trans. Smart Grid*, vol. 7, no. 2, pp. 659–668, Mar. 2016.

[5] D. Strickland, T. Embley, J. Osborne, J. Yang, Z. Qiao, A. Malhotra, A. Corliss, and K. Ashworth, "Feasibility study: Investigation of car park-based V2G services in the UK central hub," *J. Eng.*, vol. 2019, no. 17, pp. 3967–3971, Jun. 2019.

[6] G. Guidi, S. D'Arco, K. Nishikawa, and J. A. Suul, "Load balancing of a modular multilevel grid-interface converter for transformer-less large-scale wireless electric vehicle charging infrastructure," *IEEE J. Emerg. Sel. Topics Power Electron.*, vol. 9, no. 4, pp. 4587–4605, Aug. 2021.

[7] G. Guidi, S. D'Arco, J. A. Suul, R. Iso, and J. Itoh, "A modular multilevel interface for transformerless grid integration of large-scale infrastructure for wireless electric vehicle charging," in *Proc. 10th Int. Conf. Power Electron. ECCE Asia (ICPE-ECCE Asia)*, May 2019, pp. 2059–2066.

[8] G. Guidi, S. D'Arco, and J. A. Suul, "Evaluation of a modular system topology for large-scale wireless EV charging in a commercial parking facility," in *Proc. 5th Int. Electr. Vehicle Technol. Conf. (EVTeC)*, 2021, p. 7.

[9] M. Mao, Y. Ding, L. Chang, N. D. Hatziargyriou, Q. Chen, T. Tao, and Y. Li, "Multi-objective power management for EV fleet with MMC-based integration into smart grid," *IEEE Trans. Smart Grid*, vol. 10, no. 2, pp. 1428–1439, Mar. 2019.

[10] E. Gümrükcü, F. Ponci, A. Monti, G. Guidi, S. D'Arco, and J. A. Suul, "Optimal load management strategy for large electric vehicle charging stations with undersized charger clusters," *IET Electr. Syst. Transp.*, pp. 1–16, Oct. 2021, doi: 10.1049/els2.12037.

[11] S. Li and C. C. Mi, "Wireless power transfer for electric vehicle applications," *IEEE J. Emerg. Sel. Topics Power Electron.*, vol. 3, no. 1, pp. 4–17, Mar. 2015.

[12] L. Yao, W. H. Lim, and T. S. Tsai, "A real-time charging scheme for demand response in electric vehicle parking station," *IEEE Trans. Smart Grid*, vol. 8, no. 1, pp. 52–62, Jan. 2017.

[13] G. Aragon, E. Gumrukcu, V. Pandian, and O. Werner-Kytola, "Cooperative control of charging stations for an EV park with stochastic dynamic programming," in *Proc. 45th Annu. Conf. IEEE Ind. Electron. Soc. (IECON)*, Oct. 2019, pp. 6649–6654.

[14] H. M. Abdullah, A. Gastli, and L. Ben-Brahim, "Reinforcement learning based EV charging management systems—A review," *IEEE Access*, vol. 9, pp. 41506–41531, 2021.

[15] J. F. Franco, M. J. Rider, and R. Romero, "A mixed-integer linear programming model for the electric vehicle charging coordination problem in unbalanced electrical distribution systems," *IEEE Trans. Smart Grid*, vol. 6, no. 5, pp. 2200–2210, Sep. 2015.

[16] A. C. F. Sabillón, J. F. Franco, M. J. Rider, and R. Romero, "Optimal charging coordination of electric vehicles in unbalanced electrical distribution system considering vehicle-to-grid technology," in *Proc. 3rd Int. Istanbul Smart Grid Congr. Fair (ICSG)*, Apr. 2015, pp. 1–5.

[17] M. R. Islam, H. H. Lu., M. J. Hossain, and L. Li, "Compensating neutral current, vol.tage unbalance and improving voltage of an unbalanced distribution grid connected with EV and renewable energy sources," in *Proc. 22nd Int. Conf. Electr. Mach. Syst. (ICEMS)*, Aug. 2019, pp. 1–5.

[18] P. Richardson, D. Flynn, and A. Keane, "Optimal charging of electric vehicles in low-voltage distribution systems," *IEEE Trans. Power Syst.*, vol. 27, no. 1, pp. 268–279, Feb. 2012.

[19] E. Gumrukcu, F. Ponci, A. Monti, G. Guidi, S. D'Arco, and J. A. Suul, "Optimized allocation of loads in MMC-based electric vehicle charging infrastructure," in *Proc. IEEE Int. Conf. Power Syst. Technol. (POWERCON)*, Sep. 2020, pp. 1–6.

[20] L. Harnefors, A. Antonopoulos, S. Norrga, L. Ängquist, and H.-P. Nee, "Dynamic analysis of modular multilevel converters," *IEEE Trans. Ind. Electron.*, vol. 60, no. 7, pp. 2526–2537, Jul. 2013.

[21] H. Bayat and A. Yazdani, "A power mismatch elimination strategy for an MMC-based PV system in unbalanced grids," in *Proc. IEEE Electr. Power Energy Conf. (EPEC)*, Oct. 2018, pp. 1–6.

[22] T. Soong and P. W. Lehn, "Internal power flow of a modular multilevel converter with distributed energy resources," *IEEE J. Emerg. Sel. Topics Power Electron.*, vol. 2, no. 4, pp. 1127–1138, Dec. 2014.

[23] A. Lesnicar and R. Marquardt, "An innovative modular multilevel converter topology suitable for a wide power range," in *Proc. IEEE Bologna Power Tech Conf.*, Jun. 2003, p. 6.

[24] *Op5700 User Manual*. Accessed: Oct. 22, 2021. [Online]. Available: https://www.opal-rt.com/resource-center

[25] H. Akima, "A new method of interpolation and smooth curve fitting based on local procedures," *J. ACM*, vol. 17, no. 4, pp. 589–602, Oct. 1970, doi: 10.1145/321607.321609.

[26] W. E. Hart, C. D. Laird, J.-P. Watson, D. L. Woodruff, G. A. Hackebeil, B. L. Nicholson, and J. D. Siirola, *Pyomo–Optimization Modeling in Python*, vol. 67, 2nd ed. Cham, Switzerland: Springer, 2017.
[27] *IBM ILOG CPLEX*. Accessed: Sep. 1, 2021. [Online]. Available: https://www.ibm.com/de-de/products/ilog-cplex-optimization-studio

ERDEM GÜMRÜKCÜ (Graduate Student Member, IEEE) received the master's degree in electrical power engineering from RWTH Aachen University, Aachen, Germany, in 2018. He is currently pursuing the Ph.D. degree in energy flexibility management and optimization for large scale electric vehicle charging. In 2018, he joined the E.ON Energy Research Center, Institute for Automation of Complex Power Systems, RWTH Aachen University, as a Research Associate.

EHSAN ASADOLLAHI (Student Member, IEEE) received the bachelor's degree in electrical power engineering from the University of Tehran, Iran, in 2018. He is currently pursuing the master's degree in medium voltage DC circuit breakers. In 2019, he joined the E.ON Energy Research Center, Institute for Automation of Complex Power Systems, RWTH Aachen University, Aachen, Germany, as a Student Research Assistant.

CHARUKESHI JOGLEKAR (Graduate Student Member, IEEE) received the master's degree in electrical power engineering from RWTH Aachen University, Aachen, Germany, in 2018. She is currently pursuing the Ph.D. degree in resilience and interoperability of smart grids with high levels of electric mobility integration. In 2018, she joined the E.ON Energy Research Center, Institute for Automation of Complex Power Systems, RWTH Aachen University, as a Research Assistant.

FERDINANDA PONCI (Senior Member, IEEE) received the Ph.D. degree in electrical engineering from the Politecnico di Milano, Milan, Italy, in 2002. In 2003, she joined the Department of Electrical Engineering, University of South Carolina, Columbia, SC, USA, as an Assistant Professor, where she became an Associate Professor, in 2008. In 2009, she joined the E.ON Energy Research Center, Institute for Automation of Complex Power Systems, RWTH Aachen University, Aachen, Germany, where she is currently a Professor of monitoring and distributed control for power systems. Her current research interests include automation and advanced monitoring of active distribution systems.

ANTONELLO MONTI (Senior Member, IEEE) received the M.Sc. *(summa cum laude)* and Ph.D. degrees in electrical engineering from the Politecnico di Milano, Italy, in 1989 and 1994, respectively. He started his career at Ansaldo Industria and then in 1995, he moved as an Assistant Professor to the Politecnico di Milano. In 2000, he joined the Department of Electrical Engineering, University of South Carolina, USA, as an Associate Professor, and then a Full Professor. Since 2008, he has been the Director of the E.ON Energy Research Center, Institute for Automation of Complex Power Systems, RWTH Aachen University. He is the author or a coauthor of more than 300 peer-reviewed articles published in international journals and in the proceedings of international conferences. He was a recipient of the 2017 IEEE Innovation in Societal Infrastructure Award. He is an Associate Editor of the IEEE Systems Journal and *IEEE Electrification Magazine*, a member of the Editorial Board of *SEGAN* journal (Elsevier), and a member of the Founding Board of the *Energy Informatics* journal (Springer).

GIUSEPPE GUIDI (Senior Member, IEEE) received the graduate degree from the University of L'Aquila, L'Aquila, Italy, in 1995, and the Ph.D. degree from the Norwegian University of Science and Technology (NTNU), Trondheim, Norway, in 2009. He has been involving in the field of power electronic drives, since 1997, joining first at Fuji Electric Research and Development, Japan, as a Research and Development Engineer, until 2001, and then at SIEI SpA, Italy, as a Senior Engineer, until 2004. In 2009, he joined Yokohama National University, Yokohama, Japan, as a Research Associate, working on power converters for electric vehicles. From 2011 to 2013, he was a part-time Research Associate with NTNU, until joining SINTEF Energy Research, Trondheim. His current research interests include power electronics, traction control, and drive systems for electric propulsion, as well as application of power electronics to renewable energy.

SALVATORE D'ARCO received the M.Sc. and Ph.D. degrees in electrical engineering from the University of Naples "Federico II," Naples, Italy, in 2002 and 2005, respectively. From 2006 to 2007, he was a Postdoctoral Researcher at the University of South Carolina, Columbia, SC, USA. In 2008, he joined ASML, Veldhoven, The Netherlands, as a Power Electronics Designer, where he worked, until 2010. From 2010 to 2012, he was a Postdoctoral Researcher with the Department of Electric Power Engineering, Norwegian University of Science and Technology (NTNU), Trondheim, Norway. In 2012, he joined SINTEF Energy Research, where he currently works as a Senior Research Scientist. He has authored more than 100 scientific papers. He is the holder of one patent. His main research interests include control and analysis of power electronic conversion systems for power system applications, including real-time simulation and rapid prototyping of converter control systems.

JON ARE SUUL (Member, IEEE) received the M.Sc. degree in energy and environmental engineering and the Ph.D. degree in electric power engineering from the Norwegian University of Science and Technology (NTNU), Trondheim, Norway, in 2006 and 2012, respectively. From 2006 to 2007, he was with SINTEF Energy Research, Trondheim, where he was working in simulation of power electronic converters and marine propulsion systems until starting his Ph.D. studies. Since 2012, he has been a Research Scientist with SINTEF Energy Research, first in a part-time position while working as a part-time Postdoctoral Researcher with the Department of Electric Power Engineering, NTNU, until 2016. Since 2017, he has been an Adjunct Associate Professor with the Department of Engineering Cybernetics, NTNU. His research interests include modeling, analysis, and control of power electronic converters in power systems, renewable energy applications, and electrification of transport. He is an Associate Editor of the IEEE Journal of Emerging and Selected Topics in Power Electronics and the IEEE Journal of Emerging and Selected Topics in Industrial Electronics.